Materials Advances

ROYAL SOCIETY OF CHEMISTRY

PAPER

View Article Online
View Journal | View Issue

Check for updates

Cite this: *Mater. Adv.*, 2022, **3**, 2185

Preparation of heterostructured TiO_2/MoS_2 for efficient photocatalytic rhodamine B degradation†

Ping Li,‡[a] Mengyou Gao,‡[ab] Lei Sun,[a] Huizhong Xu,[a] Xiaochen Dong[c] and Jianjian Lin*[a]

Received 10th November 2021,
Accepted 9th January 2022

DOI: 10.1039/d1ma01050f

rsc.li/materials-advances

Coating a few layers of MoS_2 nanosheets on a substrate is an effective approach to enhance catalytic activity for photocatalytic degradation. Herein, we fabricated heterostructured TiO_2/MoS_2 (H-TiO_2/MoS_2) with high structural stability *via* a simple two-step solvothermal approach. H-TiO_2/MoS_2 was composed of TiO_2 as a hard core and MoS_2 nanosheets as a shell, which could increase the electron transfer rate between TiO_2 and MoS_2 and enable active edge sites of MoS_2 to be maximally exposed. Besides, H-TiO_2/MoS_2 indicated enhanced light absorption in the UV to Vis range when compared to TiO_2 nanoparticles, and slightly lower than that of MoS_2. This is beneficial for the enhancement of the photocatalytic degradation performance. Therefore, H-TiO_2/MoS_2 displayed a strong adsorption ability toward organic dyes and showed excellent performance in the photocatalytic degradation of rhodamine B with the concentration decreased by 99.4% due to the synergistically stimulative effect. The work will enlighten the development of highly efficient molybdenum sulfide-based heterostructured photocatalysts.

Introduction

Nowadays, semiconductor photocatalysts are attracting increasing attention owing to their high efficiency in easing the energy crisis and reducing environmental pollution. Recently, a large variety of semiconductor photocatalysts have been explored including TiO_2,[1,2] $SrTiO_3$,[3] *etc.*, which were mainly active in the ultraviolet range, and C_3N_4,[4] Cu_2O, Co_3O_4,[5] CdS,[6] *etc.* that have high visible light activity. TiO_2, as an n-type photocatalytic semiconductor, is efficient for the separation of electrons and holes. Furthermore, it has both good chemical and physical stability, relatively low cost and nontoxicity, and thus has a wide range of applications in various fields, such as self-cleaning and removal of hazardous compounds. However, the large band gap of TiO_2 (3.2 eV) has become the main drawback because limited UV light could be used, which significantly decreased the photocatalytic performance. Additionally, pure TiO_2 usually did not have a high charge separation rate, and therefore illustrated relatively low photocatalytic activity. Thus, many research studies have been conducted to settle these inadequacies including tuning the particle size,[7] crystallinity and morphologies (nanotubes[8] in 1D, nanosheets[9] in 2D and microspheres[10] or nanoflowers[11] in 3D), and constructing heterostructured materials,[12–14] which have resulted in the promotion of the photocatalytic performance. Among these nanostructures, heterostructures like core–shell structures[15] with a large specific surface area and matched energy levels have attracted great attention.

Moreover, it has been reported that TiO_2-based photocatalysts doped with cocatalysts like noble metals,[10] MoS_2,[16–18] *etc.*, could broaden the range of light harvesting from the UV to UV-vis, and improve the charge separation efficiency. Two-dimensional transition metal sulfides (2D MS_x), such as the typical MoS_2, were reported as platinum-like materials, which were beneficial for improving the photocatalytic performance as a cocatalyst because of great (photo) electronic and catalytic traits.[19] In addition, a few-layered MoS_2 with increased edges was beneficial for electron acceptance, as well as increased active sites, illustrating improved photocatalytic performance. Recently, MoS_2 catalysts with a variety of nanostructures have been prepared using various approaches including chemical vapour deposition,[20] thermolysis[21] or hydrothermal and solvothermal methods.[22] Irregular aggregates of nanoparticles or stacked multilayers of the as-fabricated MoS_2, however, largely limited the photocatalytic performance. Therefore, preparing heterostructured MoS_2-based photocatalysts with enhanced photocatalytic activity remains challenging. Recently, MoS_2-based photocatalysts such as CdS/MoS_2,[23,24] graphene/

---

[a] *Shandong Key Laboratory of Biochemical Analysis, College of Chemistry and Molecular Engineering, Qingdao University of Science and Technology, Qingdao 266042, P. R. China. E-mail: Jianjian_Lin@qust.edu.cn*

[b] *College of Automation and Electronic Engineering, Qingdao University of Science and Technology, Qingdao 266042, P. R. China*

[c] *Key Laboratory of Flexible Electronics (KLOFE) & Institute of Advanced Materials (IAM), Nanjing Tech University (NanjingTech), 30 South Puzhu Road, Nanjing, 211800, P. R. China*

† Electronic supplementary information (ESI) available. See DOI: 10.1039/d1ma01050f

‡ These authors equally contributed to this work

MoS_2[25,26] and TiO_2/MoS_2 heterostructures with various structures including particles[27] (0D), belts[28] and wires[12] (1D), sheets[29] (2D) and flowers[30] (3D) have demonstrated enhanced photocatalytic activities. Meanwhile, constructing novel nanostructures of core-shelled TiO_2/MoS_2 is also an effective approach to develop photocatalysts with large specific surface areas and increased active sites.

In this work, we prepared H-TiO_2/MoS_2 through a two-step solvothermal approach. In the first step, TiO_2 nanoparticles were prepared as an ellipsoidal core through a solvothermal approach; then MoS_2 nanosheets were coated on the surface of the TiO_2 precursor again using a solvothermal method. The MoS_2 nanosheets which were coated on the surface of TiO_2 nanoparticles could allow fast electron transfer between TiO_2 and MoS_2. Furthermore, H-TiO_2/MoS_2 illustrated good structural stability. MoS_2 nanosheets could expose active edge sites maximally, allowing an enhanced adsorption ability and improved photocatalytic degradation performance of rhodamine B (RhB). The synergistic effect of the novel heterostructure between MoS_2 nanosheets and TiO_2 nanoparticles accounted for the outstanding photocatalytic degradation performance.

Experimental

Chemicals

Tetrabutyl titanate (TBT, Aladdin Biochemical Technology Co., Ltd) and glacial acetic acid (Macklin Co., Ltd) were used without further purification. Absolute ethanol and $Na_2MoO_4\cdot 2H_2O$ were purchased from Sinopharm Chemical Regent Co., Ltd. Cysteine was purchased from Beijing Xinjingke Biotechnology Co., Ltd. Ultrapure H_2O was employed in all experiments.

Preparation of TiO_2

In a typical synthesis process, the TiO_2 precursor was synthesized by a hydrothermal strategy.[7,31] In detail, TBT (1 mL) was dropped into glacial acetic acid (15 mL) at room temperature, followed by addition of ultrapure water (0.3 mL) to initiate the hydrolysis of TBT. The mixture was stirred for ~10 minutes at room temperature, and then transferred into a 50 mL autoclave, which was heated at 150 °C for 12 h. The as-prepared precursor was obtained by centrifugation after cooling the autoclave to room temperature and washed thoroughly with absolute ethanol and water several times with the assistance of ultrasound treatment.

Synthesis of H-TiO_2/MoS_2

H-TiO_2/MoS_2 was prepared *via* a solvothermal method.[22] In detail, 100 mg TiO_2 was dissolved into C_2H_5OH (10 mL) and H_2O (20 mL), then $Na_2MoO_4\cdot 2H_2O$ (0.3 g) and cysteine (1.25 g) were added under vigorous stirring in sequence. Then the mixed solution was transferred into an autoclave (50 mL) and heated at 200 °C for 24 h. The resultant sample was obtained by centrifugation after cooling the autoclave to room temperature. Finally, the obtained sample was washed thoroughly with absolute ethanol and water several times with the assistance of ultrasound treatment. The as-fabricated H-TiO_2/MoS_2 was heated at 800 °C (5 °C min^{-1}) under an Ar (5% H_2) atmosphere for 2 h before collection.

Characterization

X-Ray diffraction (Bruker D8 Advance) with Ni-filtered Cu Kα radiation was used to reveal the crystal structure of the as-prepared samples at 40 kV and 40 mA with a step size of 0.02° and scan speed of 0.1 s. Transmission electron microscopy (TEM, FEI Tecnai G2 F20) and scanning electron microscopy (SEM, Zeiss Merlin compact LE0 1530 VP) were used to explore the morphologies and elemental compositions of the as-prepared samples. The Raman spectrum of TiO_2/MoS_2 was recorded on an Invia Qontor. Fourier transform-infrared (FT-IR) spectroscopy was performed to confirm the spectrum of TiO_2/MoS_2 in the range of 400–4000 cm^{-1} using a PerkinElmer Spectrum One spectrometer. N_2 adsorption and desorption curves were obtained for the analysis of pore structure by ASAP 2460. UV-Vis absorption spectra were recorded on a PerkinElmer (Lambda 1050 +) for revealing the light absorption of the as-prepared samples.

Photocatalytic degradation measurement

Photocatalytic activity was studied at room temperature by the degradation of RhB using a 300 W Xe lamp. For the photocatalytic test, 50 mL of an aqueous suspension of RhB (15 mg L^{-1}) and 5 mg of the samples were placed in a Pyrex glass tube. Before irradiation, the suspension was sonicated and stirred for 30 min in the dark. The mixed solution was continuously stirred during the photocatalytic reaction. During the photocatalytic reaction process, 3 mL of the suspension were collected after irradiation for the following analysis after the filtration. The concentration of RhB was monitored by measuring the absorbance at 554 nm using a UV-vis spectrometer (Lambda 1050 +). Isopropanol, DMSO and *t*-BuOH were used as free radical scavengers for the scavenging experiments. The pH values of RhB solution were controlled by 0.1 M HCl and 0.1 M NaOH.

Results and discussion

Morphology and composition

As illustrated in Scheme 1, H-TiO_2/MoS_2 was fabricated *via* a simple two-step method. Initially, the porous TiO_2 (rice-like) precursor was prepared *via* a facile solvothermal method;[7,31] then the TiO_2 precursor was seen as a hard core, which loaded MoS_2 as a shell outside, resulting in the successful preparation of H-TiO_2/MoS_2. Firstly, the tetrabutyl titanate precursor was hydrolyzed and nucleated into TiO_2 microcrystals, and then the microcrystals gradually grew as porous TiO_2. In detail, the tetrabutyl titanate precursor was hydrolyzed into numerous winding chain bundles after 2 h of reaction (Fig. S1a, ESI†). As the reaction proceeds, some chain bundles are gradually rotated and twisted into ellipsoidal aggregates which can serve as crystal nuclei.[31] Finally, after 12 h of reaction, all the

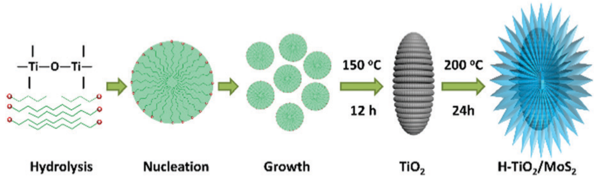

Scheme 1 Scheme of the preparation process for as-prepared H-TiO_2/MoS_2.

ellipsoidal aggregates grew into ellipsoidal particles (Fig. S1b, ESI†). The H-TiO_2/MoS_2 heterostructure was formed by an L-cysteine-assisted method.[22,32] For the self-assembly process of the H-TiO_2/MoS_2 heterostructure, the porous TiO_2 served as a precursor core for the adsorption of $MoO_4{}^{2-}$ anions. When heated in the solution-phase reaction, L-cysteine can release H_2S, meanwhile acting as a sulfide source and a reducing agent.[32] As the reaction time increased, H_2S *in situ* reacted with $MoO_4{}^{2-}$ anions to form a two-dimensional nano-plate-like structure, which is common in other MoS_2-based composites.[33–35] As illustrated in Fig. S2 (ESI†), MoS_2 can be loaded onto the surface of TiO_2 in a short time and gradually crystallize with time.

As shown in X-ray diffraction patterns of Fig. 1, the crystal structure of the as-prepared precursor can be confirmed as TiO_2 (anatase, Fig. S3a, ESI,† JCPDS No. 21-1272).[7,31] Besides, the crystal structure of the resultant sample was confirmed to be H-TiO_2/MoS_2, which corresponds to TiO_2 and MoS_2 (2H, Fig. S3b, ESI,† JCPDS No. 37-1492)[22] phases, indicating that H-TiO_2/MoS_2 was fabricated successfully.

To indicate the porous structure of TiO_2, the characterization studies including magnified SEM and TEM images and N_2 adsorption and desorption curves of a single TiO_2 particle were performed. As illustrated in Fig. S4a and b (ESI†), the SEM and TEM images showed that the TiO_2 particle had plenty of pores, and the N_2 adsorption and desorption curves demonstrated a specific surface area of 103.07 $m^2\ g^{-1}$ for TiO_2 particles (Fig. S4c, ESI†).

The morphology of H-TiO_2/MoS_2 (~240 nm) was confirmed by SEM and TEM. The SEM image in Fig. 2a illustrated that MoS_2 nanosheets (~20 nm thickness) were coated on the surface of TiO_2 nanoparticles successfully, which matched well with the TEM image in Fig. 2b. Additionally, the single magnified particle in Fig. 2c clearly showed that a few layer MoS_2 (~10–30 layers) was loaded onto the surface of TiO_2. What is more, as illustrated in the high-resolution TEM (HRTEM) image of Fig. 2d, the lattice fringe of 0.35 nm corresponded to the (101) plane of TiO_2, and a lattice fringe of 0.6 nm corresponded to the (002) facet of MoS_2.[36] In order to explore the element dispersion of H-TiO_2/MoS_2, scanning transmission electron microscopy energy dispersive spectroscopy (STEM EDS) was employed. As shown in Fig. 2e–i, Ti and O were distributed evenly inside as a core, while Mo and S were located outside as a shell, demonstrating that MoS_2 encapsulated on the surface of TiO_2 successfully, which was consistent with SEM and TEM results.

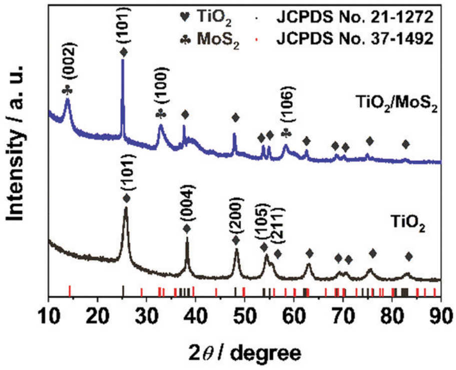

Fig. 1 XRD patterns of as-prepared TiO_2 and H-TiO_2/MoS_2.

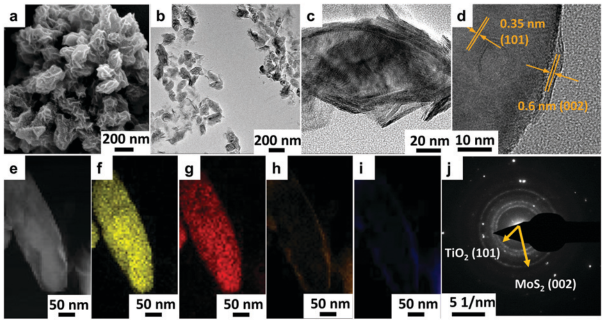

Fig. 2 (a) SEM, (b) low- and (c) high-magnification TEM image, (d) HRTEM image, (e–i) STEM EDS mapping images and (j) SAED image of H-TiO_2/MoS_2.

Furthermore, the selected area electron diffraction (SAED) pattern in Fig. 2j pointed to the TiO_2 (101) facet and MoS_2 (002) facet, and corresponds well with the HRTEM image in Fig. 2d.

The rice-like morphology of the as-fabricated TiO_2 is clearly shown in Fig. 3a with ~200 nm in length and ~70 nm in width. Meanwhile, MoS_2 flowers were prepared and are shown in the SEM image in Fig. 3b.

The Raman scattering spectrum in Fig. 4a illustrated a series of Raman peaks of the as-prepared H-TiO_2/MoS_2, which corresponded to the typical peaks of MoS_2 and TiO_2. The peak located at 379 cm^{-1} was attributed to the in-plane E^1_{2g} mode, while the peak located at 404 cm^{-1} was ascribed to the out-of-plane A_{1g} mode of MoS_2.[37] Meanwhile, the Raman peak located at 144 cm^{-1} corresponded to the E_{1g} mode of TiO_2. The FT-IR spectrum of the as-prepared H-TiO_2/MoS_2 is shown in Fig. 4b. There are broad bands of H-TiO_2/MoS_2 at 486 cm^{-1}, 903 cm^{-1}, 1122 cm^{-1}, and 1640 cm^{-1}.[38] The band which was located at

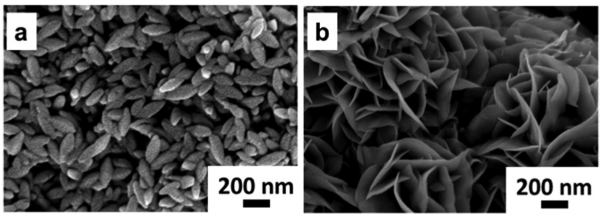

Fig. 3 SEM images of (a) TiO_2 nanoparticles and (b) MoS_2 flowers.

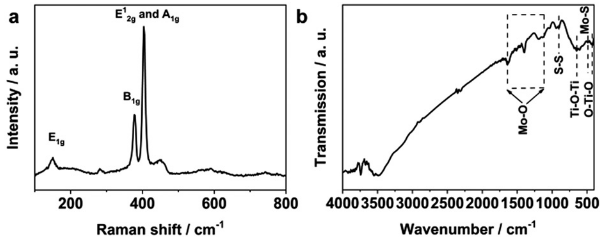

Fig. 4 Raman and FTIR spectra of as-prepared H-TiO_2/MoS_2.

486 cm^{-1} corresponded to the Mo–S bond, while the band situated at 903 cm^{-1} was assigned to the S–S bond. The bands between 1122 cm^{-1} and 1640 cm^{-1} were ascribed to the stretching vibrations of –OH and Mo–O.

Photo absorption and photocatalytic degradation of RhB

UV-Vis absorption spectra were obtained to understand the optical properties. As illustrated in Fig. S5 (ESI†), H-TiO_2/MoS_2 showed enhanced light absorption in the UV to Vis range when compared to TiO_2 nanoparticles, which is slightly lower than that of MoS_2. The photocatalytic degradation of RhB for H-TiO_2/MoS_2 was evaluated under a 300 W Xe lamp (Fig. 5a). Before light irradiation, the photocatalyst went through an adsorption process in RhB solution in the dark for 30 min. Interestingly, it is found that H-TiO_2/MoS_2 illustrated a stronger adsorption ability towards RhB than TiO_2 nanoparticles and MoS_2 flowers, which was reported have an efficient photocatalytic performance. In addition, the RhB photodegradation efficiency of H-TiO_2/MoS_2 was greater than that of TiO_2 nanoparticles and slightly higher than that of MoS_2 flowers, suggesting the advantages of H-TiO_2/MoS_2 nanostructures. Specifically, the concentrations of RhB were decreased by 32.6%, 36.2%, and 29.6% after irradiation with catalyst of H-TiO_2/MoS_2, TiO_2 nanoparticles, and MoS_2 flowers, respectively. It is remarkable that the concentration of RhB decreased by 99.4% using H-TiO_2/MoS_2, which was beneficial for RhB adsorption and degradation. As shown in Fig. 5b, the recycling stability of H-TiO_2/MoS_2 was tested for 5 cycles, and illustrated no evident decay, which demonstrated a good stability.

Additionally, as illustrated in Fig. S6 (ESI†), the consumed time for degradation decreased as the pH value increased. Specifically, it only took 20 min for RhB degradation at pH = 3, while it took ~50 min for RhB degradation at pH = 6.9 and 8.9. This indicated that the degradation of RhB was easier in acid solution.

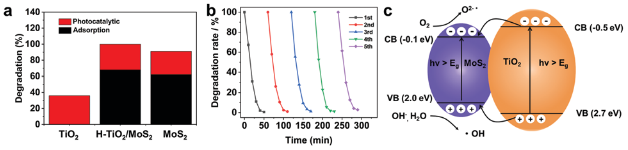

Fig. 5 (a) Adsorption of RhB in dark (30 min) and photocatalytic degradation of RhB under the light irradiation (40 min) with TiO_2 nanoparticles, H-TiO_2/MoS_2 and MoS_2 flowers. (b) The recycling stability and (c) schematic photocatalytic degradation principle of H-TiO_2/MoS_2.

The schematic diagram (Fig. 5c) illustrates the energy band structure of H-TiO_2/MoS_2 and the process of electron transfer and the formation process of reactive oxygen species. Generally, the band gap of TiO_2 (anatase) was relatively wide (~3.2 eV), while the band gap of MoS_2 was narrower (~1.8 eV).[39] Upon light illumination, electrons could be excited from the valence band (VB) of MoS_2 to the conduction band (CB), leaving holes in the VB. Compared with TiO_2, it was easy to induce photo-generated electrons in MoS_2 with a relatively lower CB, and the photo-induced electrons (CB, MoS_2) could rapidly transport to TiO_2 nanoparticles (CB). The Mott–Schottky test was carried out to determine the flat-band potential of H-TiO_2/MoS_2.[40] As illustrated in Fig. S7 (ESI†), the potential can be confirmed to be ~−0.47 V (*vs.* SCE). The corresponding potential was converted to 0.18 V (*vs.* RHE) according to the equation E (*vs.* RHE) = E (*vs.* SCE) + 0.0591 pH + 0.244 V. Owing to dissolved oxygen in solution, photo-induced electrons could form superoxide radical anions from trapped O_2 ($O_2 + e^- \rightarrow O^{2-\bullet}$), $O^{2-\bullet}$, as a high activity intermediate, usually used to degrade organic pollutants. On the valence band, the leaving holes were transferred from TiO_2 to MoS_2 due to the higher VB, H_2O was oxidized into hydroxyl radicals by holes with strong reduction ($H_2O + h^+ \rightarrow {}^\bullet OH$), which could oxidize organic dye into CO_2 and H_2O, *etc.*[41] The active species generated in the process of photodegradation were h^+, radical $O_2^\bullet$ and radical $^\bullet OH$.[42] In order to reveal the main active species that played the significant role in the photodegradation of RhB, the free radical scavenging experiments were conducted. In detail, free radical scavengers of isopropanol, dimethylsulfoxide (DMSO) and *t*-BuOH were added to the photodegradation system as a h^+ trapping agent, a radical $O_2^{\bullet -}$ trapping agent and a radical $OH^\bullet$ trapping agent, respectively. As illustrated in Fig. S8 (ESI†), the photodegradation efficiency of RhB without adding a trapping agent was 94.7%, and the degradation efficiencies after adding isopropanol, *t*-BuOH and DMSO were 97.0%, 78.5% and 25.4%, respectively. The photodegradation performance of RhB was inhibited notably after adding DMSO, which confirmed that radical $O_2^{\bullet -}$ was the main active species used for oxidation and h^+ played a synergistic role in the photocatalytic reaction,[43] and radical $^\bullet OH$ indicated no evident effect.[44] H-TiO_2/MoS_2 was just tapping into its strong charge separation ability and weak charge–hole recombination ability for enhancing the photocatalytic degradation performance.

Conclusions

H-TiO_2/MoS_2 consisting of TiO_2 as a hard core and MoS_2 as a shell was prepared through a facile two-step solvothermal approach. H-TiO_2/MoS_2 was beneficial for fast electron transfer between TiO_2 and MoS_2 due to maximally exposed active edge sites of MoS_2 and illustrated high structural stability. Moreover, H-TiO_2/MoS_2 indicated enhanced light absorption and improved performance in the photocatalytic degradation of RhB (99.4%). The synergistic effect between MoS_2 nanosheets and TiO_2 nanoparticles accounted for the outstanding photocatalytic degradation performance. Therefore, this novel photocatalyst is promising for preparing elaborate heterostructures and applications in various fields, such as sewage-treatment, dye degradation, *etc.*

Author contributions

Ping Li: data curation, writing – original draft, methodology, investigation. Mengyou Gao: supervision, writing – review and editing. Lei Sun: investigation, data curation. Huizhong Xu: data curation. Xiaochen Dong: methodology, investigation. Jianjian Lin: methodology, conceptualization, supervision, writing – review and editing.

Conflicts of interest

The authors declare that there are no conflicts to declare.

Acknowledgements

This work was partly supported by QUSTHX201919. J. Lin is supported by the Young Taishan Scholarship Project of Shandong Province (tsqn201909115).

Notes and references

1 A.-Y. Zhang, W.-Y. Wang, J.-J. Chen, C. Liu, Q.-X. Li, X. Zhang, W.-W. Li, Y. Si and H.-Q. Yu, Epitaxial Facet Junctions on TiO_2 Single Crystals for Efficient Photocatalytic Water Splitting, *Energy Environ. Sci.*, 2018, **11**, 1444–1448.

2 W. Zhang, H. He, Y. Tian, K. Lan, Q. Liu, C. Wang, Y. Liu, A. Elzatahry, R. Che, W. Li and D. Zhao, Synthesis of Uniform Ordered Mesoporous TiO_2 Microspheres with Controllable Phase Junctions for Efficient Solar Water Splitting, *Chem. Sci.*, 2019, **10**, 1664–1670.

3 L. Mu, Y. Zhao, A. Li, S. Wang, Z. Wang, J. Yang, Y. Wang, T. Liu, R. Chen, J. Zhu, F. Fan, R. Li and C. Li, Enhancing Charge Separation on High Symmetry $SrTiO_3$ Exposed with Anisotropic Facets for Photocatalytic Water Splitting, *Energy Environ. Sci.*, 2016, **9**, 2463–2469.

4 L. Ai, R. Shi, J. Yang, K. Zhang, T. Zhang and S. Lu, Efficient Combination of g-C_3N_4 and CDs for Enhanced Photocatalytic Performance: A Review of Synthesis, Strategies, and Applications, *Small*, 2021, 2007523.

5 L. Wang, J. Wan, Y. Zhao, N. Yang and D. Wang, Hollow Multi-Shelled Structures of Co_3O_4 Dodecahedron with Unique Crystal Orientation for Enhanced Photocatalytic CO_2 Reduction, *J. Am. Chem. Soc.*, 2019, **141**, 2238–2241.

6 R. Shen, D. Ren, Y. Ding, Y. Guan, Y. H. Ng, P. Zhang and X. Li, Nanostructured CdS for Efficient Photocatalytic H_2 Evolution: A Review, *Sci. China Mater.*, 2020, **63**, 2153–2188.

7 J. Lin, P. Li, H. Xu, Y. Kim, Z. Jing and D. Zheng, Controlled Synthesis of Mesoporous Single-Crystalline TiO_2 Nanoparticles for Efficient Photocatalytic H_2 Evolution, *J. Hazard. Mater.*, 2020, **391**, 122530.

8 P. Petrisková, O. Monfort, L. Satrapinskyy, E. Dobročka, T. Plecenik, G. Plesch, R. Papšík, R. Bermejo and Z. Lenčéš, Preparation and Photocatalytic Activity of TiO_2 Nanotube Arrays Prepared on Transparent Spinel Substrate, *Ceram. Int.*, 2021, **47**, 12970–12980.

9 X. Tao, P. Ruan, X. Zhang, H. Sun and X. Zhou, Microsphere Assembly of TiO_2 Mesoporous Nanosheets with Highly Exposed (101) Facets and Application in a Light-Trapping Quasi-Solid-State Dye-Sensitized Solar Cell, *Nanoscale*, 2015, **7**, 3539–3547.

10 Z. Jiang, W. Wei, D. Mao, C. Chen, Y. Shi, X. Lv and J. Xie, Silver-Loaded Nitrogen-Doped Yolk-Shell Mesoporous TiO_2 Hollow Microspheres with Enhanced Visible Light Photocatalytic Activity, *Nanoscale*, 2015, **7**, 784–797.

11 Y. Liu, K. Lan, S. Li, Y. Liu, B. Kong, G. Wang, P. Zhang, R. Wang, H. He, Y. Ling, A. M. Al-Enizi, A. A. Elzatahry, Y. Cao, G. Chen and D. Zhao, Constructing Three-Dimensional Mesoporous Bouquet-Posy-like TiO_2 Superstructures with Radially Oriented Mesochannels and Single-Crystal Walls, *J. Am. Chem. Soc.*, 2017, **139**, 517–526.

12 X. Li, W. Li, M. Li, P. Cui, D. Chen, T. Gengenbach, L. Chu, H. Liu and G. Song, Glucose-Assisted Synthesis of the Hierarchical TiO_2 Nanowire@MoS_2 Nanosheet Nanocomposite and Its Synergistic Lithium Storage Performance, *J. Mater. Chem. A*, 2015, **3**, 2762–2769.

13 Y. Sun, H. Lin, C. Wang, Q. Wu, X. Wang and M. Yang, Morphology-Controlled Synthesis of TiO_2/MoS_2 Nanocomposites with Enhanced Visible-Light Photocatalytic Activity, *Inorg. Chem. Front.*, 2018, **5**, 145–152.

14 Q. Wang, P. Yu, L. Bai, R. Bao, N. Wang, C. Cheng, Z. Liu, M. Yang, W. Yang and Z. Guo, Self-Assembled Nano-Leaf/Vein Bionic Structure of TiO_2/MoS_2 Composites for Photoelectric Sensors, *Nanoscale*, 2017, **9**, 18194–18201.

15 R. Dai, A. Zhang, Z. Pan, A. M. Al-Enizi, A. A. Elzatahry, L. Hu and G. Zheng, Epitaxial Growth of Lattice-Mismatched Core-Shell TiO_2@MoS_2 for Enhanced Lithium-Ion Storage, *Small*, 2016, **12**, 2792–2799.

16 J. Liang, C. Wang, P. Zhao, Y. Wang, L. Ma, G. Zhu, Y. Hu, Z. Lu, Z. Xu, Y. Ma, T. Chen, Z. Tie, J. Liu and Z. Jin, Interface Engineering of Anchored Ultrathin TiO_2/MoS_2 Heterolayers for Highly-Efficient Electrochemical Hydrogen Production, *ACS Appl. Mater. Interfaces*, 2018, **10**, 6084–6089.

17 Q. Xiang, J. Yu and M. Jaroniec, Synergetic Effect of MoS_2 and Graphene as Cocatalysts for Enhanced Photocatalytic H_2 Production Activity of TiO_2 Nanoparticles, *J. Am. Chem. Soc.*, 2012, **134**, 6575–6578.

18 L. Zheng, S. Han, H. Liu, P. Yu and X. Fang, Hierarchical MoS_2 Nanosheet@TiO_2 Nanotube Array Composites with Enhanced Photocatalytic and Photocurrent Performances, *Small*, 2016, **12**, 1527–1536.

19 B. Chen, Y. Meng, J. Sha, C. Zhong, W. Hu and N. Zhao, Preparation of MoS_2/TiO_2 based Nanocomposites for Photocatalysis and Rechargeable Batteries: Progress, Challenges, and Perspective, *Nanoscale*, 2017, **10**, 34–68.

20 J. Zheng, X. Yan, Z. Lu, H. Qiu, G. Xu, X. Zhou, P. Wang, X. Pan, K. Liu and L. Jiao, High-Mobility Multilayered MoS_2

Flakes with Low Contact Resistance Grown by Chemical Vapor Deposition, *Adv. Mater.*, 2017, **29**, 1604540.

21 T.-Y. Chen, Y.-H. Chang, C.-L. Hsu, K.-H. Wei, C.-Y. Chiang and L.-J. Li, Comparative Study on MoS_2 and WS_2 for Electrocatalytic Water Splitting, *Int. J. Hydrogen Energy*, 2013, **38**, 12302–12309.

22 Q. Pang, Y. Zhao, X. Bian, Y. Ju, X. Wang, Y. Wei, B. Liu, F. Du, C. Wang and G. Chen, Hybrid Graphene@MoS_2@TiO_2 Microspheres for Use as a High Performance Negative Electrode Material for Lithium Ion Batteries, *J. Mater. Chem. A*, 2017, **5**, 3667–3674.

23 Y. Liu, H. Niu, W. Gu, X. Cai, B. Mao, D. Li and W. Shi, In situ Construction of Hierarchical CdS/MoS_2 Microboxes for Enhanced Visible-Light Photocatalytic H_2 Production, *Chem. Eng. J.*, 2018, **339**, 117–124.

24 L. Zhao, T. Dong, J. Du, H. Liu, H. Yuan, Y. Wang, J. Jia, H. Liu and W. Zhou, Synthesis of CdS/MoS_2 Nanooctahedrons Heterostructure with a Tight Interface for Enhanced Photocatalytic H_2 Evolution and Biomass Upgrading, *Sol. RRL*, 2021, **5**, 2000415.

25 M. Yang, L. Wang, G. Hu, X. Chen, P. L. Gong, X. Cong, Y. Liu, Y. Yang, X. Li, X. Zhao and X. Liu, Optical Identification of Interlayer Coupling of Graphene/MoS_2 van der Waals Heterostructures, *Nano Res.*, 2021, **14**, 2241–2246.

26 W. Zhou, K. Zhou, D. Hou, X. Liu, G. Li, Y. Sang, H. Liu, L. Li and S. Chen, Three-Dimensional Hierarchical Frameworks Based on MoS_2 Nanosheets Self-Assembled on Graphene Oxide for Efficient Electrocatalytic Hydrogen Evolution, *ACS Appl. Mater. Interfaces*, 2014, **6**, 21534–21540.

27 X. Liu, Z. Xing, H. Zhang, W. Wang, Y. Zhang, Z. Li, X. Wu, X. Yu and W. Zhou, Fabrication of 3D Mesoporous Black TiO_2/MoS_2/TiO_2 Nanosheets for Visible-Light-Driven Photocatalysis, *ChemSusChem*, 2016, **9**, 1118–1124.

28 W. Zhou, Z. Yin, Y. Du, X. Huang, Z. Zeng, Z. Fan, H. Liu, J. Wang and H. Zhang, Synthesis of Few-Layer MoS_2 Nanosheet-Coated TiO_2 Nanobelt Heterostructures for Enhanced Photocatalytic Activities, *Small*, 2013, **9**, 140–147.

29 Y. Yuan, Z. Ye, H. Lu, B. Hu, Y. Li, D. Chen, J. Zhong, Z. Yu and Z. Zou, Constructing Anatase TiO_2 Nanosheets with Exposed (001) Facets/Layered MoS_2 Two-Dimensional Nanojunctions for Enhanced Solar Hydrogen Generation, *ACS Catal.*, 2015, **6**, 532–541.

30 K. He, Q. Wen, C. Wang, B. Wang, S. Yu, C. Hao and K. Chen, A Facile Synthesis of Hierarchical Flower-Like TiO_2 Wrapped with MoS_2 Sheets Nanostructure for Enhanced Electrorheological Activity, *Chem. Eng. J.*, 2018, **349**, 416–427.

31 J. Lin, L. Zhao, Y. Heo, L. Wang, F. Bijarbooneh, A. Mozer, A. Nattestad, Y. Yamauchi, S. Dou and J. Kim, Mesoporous Anatase Single Crystals for Efficient $Co^{(2+/3+)}$-Based Dye-Sensitized Solar Cells, *Nano Energy*, 2015, **11**, 557–567.

32 K. Chang and W. Chen, L-Cysteine-Assisted Synthesis of Layered MoS_2/Graphene Composites with Excellent Electrochemical Performances for Lithium Ion Batteries, *ACS Nano*, 2011, **5**, 4720–4728.

33 Q. Zhou, W. Li, M. Gao, H. Xu, Y. Guo, L. Sun, D. Zheng and J. Lin, A. Truncated Octahedron Metal-Organic Framework Derived TiO_2@C@MoS_2 Composite with Superior Lithium-Ion Storage Properties, *J. Power Sources*, 2022, **518**, 230746.

34 J. Yang, L. Yu, B. Zheng, N. Li, J. Xi and X. Qiu, Carbon Microtube Textile with MoS_2 Nanosheets Grown on Both Outer and Inner Walls as Multifunctional Interlayer for Lithium–Sulfur Batteries, *Adv. Sci.*, 2020, **7**, 1903260.

35 S. Wang, B. Guan, L. Yu and X. (David), Lou, Rational Design of Three-Layered TiO_2@Carbon@MoS_2 Hierarchical Nanotubes for Enhanced Lithium Storage, *Adv. Mater.*, 2017, **29**, 1702724.

36 J. Pei, H. Geng, E. H. Ang, L. Zhang, X. Cao, J. Zheng and H. Gu, Controlled Synthesis of Hollow C@TiO_2@MoS_2 Hierarchical Nanospheres for High-Performance Lithium-Ion Batteries, *Nanoscale*, 2018, **10**, 17327–17334.

37 B. Guo, K. Yu, H. Fu, Q. Hua, R. Qi, H. Li, H. Song, S. Guo and Z. Zhu, Firework-Shaped TiO_2 Microspheres Embedded with Few-Layer MoS_2 as an Anode Material for Excellent Performance Lithium-Ion Batteries, *J. Mater. Chem. A*, 2015, **3**, 6392–6401.

38 S. V. P. Vattikuti and C. Byon, Synthesis and Characterization of Molybdenum Disulfide Nanoflowers and Nanosheets: Nanotribology, *J. Nanomater.*, 2015, **2015**, 1–11.

39 X. Hu, H. Zhao, J. Tian, J. Gao, Y. Li and H. Cui, Synthesis of Few-Layer MoS_2 Nanosheets-Coated TiO_2 Nanosheets on Graphite Fibers for Enhanced Photocatalytic Properties, *Sol. Energy Mater. Sol. Cells*, 2017, **172**, 108–116.

40 Q. Zhang, Y. Wang, X. Zhu, X. Liu and H. Li, 1T and 2H Mixed Phase MoS_2 Nanobelts Coupled with Ti^{3+} Self-Doped TiO_2 Nanosheets for Enhanced Photocatalytic Degradation of RhB under Visible Light, *Appl. Surf. Sci.*, 2021, **556**, 149768.

41 H. Yan, L. Liu, R. Wang, W. Zhu, X. Ren, L. Luo, X. Zhang, S. Luo, X. Ai and J. Wang, Binary Composite MoS_2/TiO_2 Nanotube Arrays as a Recyclable and Efficient Photocatalyst for Solar Water Disinfection, *Chem. Eng. J.*, 2020, **401**, 126052.

42 Z. Li, F. Cao, L. Wang, Z. Chen and X. Ji, A Novel Ternary MoS_2/MoO_3/TiO_2 Composite for Fast Photocatalytic Degradation of Rhodamine B under Visible-Light Irradiation, *New J. Chem.*, 2020, **44**, 537–542.

43 D. Cao, Q. Wang, S. Zhu, X. Zhang, Y. Li, Y. Cui, Z. Xue and S. Gao, Hydrothermal Construction of Flower-Like MoS_2 on TiO_2 NTs for Highly Efficient Environmental Remediation and Photocatalytic Hydrogen Evolution, *Sep. Purif. Technol.*, 2021, **265**, 118463.

44 M. Mohamed and N. Karunakaran, One-Step Solvothermal Synthesis of Carbon Doped TiO_2–MoS_2 Heterostructure Composites with Improved Visible Light Catalytic Activity, *New J. Chem.*, 2016, **40**, 8123–8130.